High-risk pathological subtype associated FAM83A-AS1 promotes malignancy and glycolysis of lung adenocarcinoma via miR-202-3p/HK2 axis

XINKUI XIONG[1*], LEI ZHANG[2*], BAO ZANG[1], DAFU XU[1], CHEN CHEN[1], GAOCHAO DONG[3], WENJIE XIA[3] and YANHU WU[4]

[1]Department of Thoracic Surgery, The Affiliated Huaian No. 1 People's Hospital of Nanjing Medical University, Huaiyin, Huaian, Jiangsu 223001; [2]Department of Medical Oncology, Xuzhou Central Hospital, Quanshan, Xuzhou 221000; [3]Department of Thoracic Surgery, Nanjing Medical University Affiliated Cancer Hospital & Jiangsu Cancer Hospital & Jiangsu Institute of Cancer Research, Nanjing; [4]Department of Cardiovascular Surgery, The First Affiliated Hospital of Nanjing Medical University, Nanjing, Jiangsu 210000, P.R. China

Received August 13, 2022; Accepted December 19, 2022

DOI: 10.3892/or.2023.8532

Abstract. According to the diverse cellular morphology, lung adenocarcinoma (LUAD) was classified into five pathological subtypes, referred to as follows: High-risk group (micropapillary and solid), intermediate-risk group (acinar and papillary) and low-risk group (epidic). Nevertheless, little is known about the biological function of long non-coding RNA (lncRNA) in the molecular determination of LUAD histologic patterns. Screening the transcriptional expression data from TCGA-LUAD, the differentially expressed lncRNA across the divergent pathological subtypes were explored. Pan-cancer analysis revealed the characteristic of FAM83A-AS1, which was also confirmed in the LUAD tissues. The function of FAM83A-AS1 was uncovered through the *in vitro* assays. RNA immunoprecipitation and dual-luciferase reporter assays were performed to explore the molecular mechanisms of FAM83A-AS1. In the present study, it was identified that the expression of FAM83A-AS1 was increased from the low-risk group to the high, which was associated with a poorer prognosis and higher risk of recurrence. Pan-cancer analysis revealed that FAM83A-AS1 was positively correlated with high tumor mutational burden. Additionally, FAM83A-AS1 promoted cell migration, invasion and growth of LUAD cancer cells. Mechanistically, FAM83A-AS1 sponged miR-202-3p to regulate the expression of hexokinase II (HK2) in post-transcription, which facilitated the malignancy and glycolysis. The present study uncovered the biological roles of FAM83A-AS1/miR-202-3p/HK2 axis in regulating malignancy and glycolysis of LUAD, which provided novel avenues to addressing the determination of histologic patterns.

Correspondence to: Professor Yanhu Wu, Department of Cardiovascular Surgery, The First Affiliated Hospital of Nanjing Medical University, 300 Guangzhou Road, Nanjing, Jiangsu 210000, P.R. China
E-mail: docwuyanhu@163.com

*Contributed equally

Key words: lung adenocarcinoma, FAM83A-AS1, histological pathology subtype, hexokinase II, glycolysis

Introduction

Lung cancer is the leading cause of death worldwide, the main type of which is lung adenocarcinoma (LUAD) (1). The robust intratumoral heterogeneity of LUAD has received wide attention, that is associated with limited therapeutic, therapeutic resistance and refractory metastasis (2). To address this serious question, a histologic subtype classification system has been proposed in 2011, which refers to lepidic (LEP), acinar (ACI), papillary (PAP), micropapillary (MIP) and solid (SOL) (3). According to the clinicopathologic characteristics and patient prognosis of these five main pathological subtypes, tumors with predominant histologic subtype were classified into three groups: a low-risk group containing LEP, an intermediate-risk group containing ACI and PAP and a high-risk group containing MIP and SOL (4).

LncRNA is a class of transcripts originating from non-protein coding genome regions with a length of >200 nucleotides (5). Increasing evidence indicates that lncRNAs are widely expressed in tissues and play important roles in various physiological and pathological processes by regulating activation and suppression of transcription, RNA sponging, degradation, apoptosis, proliferation, epigenetic modifications and chromatin remodeling (6). Li *et al* (7) revealed that lncRNA lnc-APUE promotes G1/S phase transition and tumor growth in hepatocellular carcinoma (HCC) by acting as a miR-20b sponge. Dysregulation of lncRNAs has been reported to involve in the malignant progression of numerous kinds of cancer (8). For instance, lncRNA Smyca drives multiple tumor progression and therapy resistance

by coactivating the TGF-β/Smad and c-Myc pathways (9). Moreover, the potential mechanism of lncRNAs in multiple tumor metabolic regulation processes is a hot topic of research. It has been demonstrated that lncRNAs regulate glycolysis in different types of cancer. Ma *et al* (10) reported that LncRNA FGF13-AS1 impairs glycolysis and stemness properties via the FGF13-AS1/IGF2BPs/Myc feedback loop to inhibit the malignant progression of breast cancer. To the best of our knowledge, however, an investigation of lncRNA has not yet been reported to address the molecular mechanism of histologic patterns.

In the present study, our group first downloaded LUAD pathological H&E from The Cancer Genome Atlas (TCGA) as well as the transcriptional expression data. According to the annotation label, lncRNA expression data in the three risk groups of different pathological subtypes were pairwise compared. Overlapping the differentially expressed lncRNAs between the three histological pathology risk groups, and between tumor tissues and adjacent normal tissues of LUAD (Fig. 1A), focus was addressed on the candidate lncRNA, FAM83A-AS1, which was associated with poorer prognosis and higher risk of recurrence. Pan-cancer analysis revealed that FAM83A-AS1 was positively correlated with high tumor mutational burden (TMB) in LUAD. Functional assays identified that FAM83A-AS1 promoted cell migration and invasion and growth in LUAD cancer cell lines. Mechanistically, FAM83A-AS1 sponged miR-202-3p to regulate the expression of hexokinase II (HK2) in post-transcription, which facilitated the malignancy and glycolysis. The present study identified that FAM83A-AS1 was positively associated with high-risk pathological subtype and higher clinical stages, and emphasized the biological roles of FAM83A-AS1/miR-202-3p/HK2 axis in regulating malignancy and glycolysis of LUAD, which provided a novel avenue to address the molecular mechanism of histologic patterns.

Materials and methods

Clinical samples. For the present study, 40 tumor and paired normal tissues were obtained from patients (Age, 40-75; sex, 28 males and 12 females) who underwent surgery in the Department of Thoracic Surgery of Jiangsu Cancer Hospital (Nanjing, China) from July 2020 to December 2021 (Table I). An area of 0.5 cm^3 in the center of the tumor and a paired normal tissue 5 cm from the edge of the tumor were selected. None of the patients had received chemotherapy or immunotherapy before surgery. After being promptly frozen in liquid nitrogen, all tissues were kept at -80˚C. The present study was approved (approval no. IACUC-2017088-1) by the Ethics Committee of the The First Affiliated Hospital of Nanjing Medical University (Nanjing, China) and complied with the ethical standards of the institution. Written informed consent was provided by all enrolled participants.

Cell culture and treatment. Short tandem repeat sequence analysis was used to identify all cell lines (HBE, A549, H358, SW1573, H1975 and PC9) that were purchased from the Shanghai Institute of Cell Biology, Chinese Academy of Sciences. All cell lines were cultured in a humidified atmosphere supplemented with 5% CO_2 at 37˚C.

Dataset. Gene expression (transcripts per million) data and associated clinical information were downloaded from TCGA (http://cancergenome.nih.gov/; https://portal.gdc.cancer.gov/projects/TCGA-LUAD). DNA methylation dataset (Illumina Human Methylation 450K BeadChip Kit) and LUAD pathological H&E-stained whole-slide images were also downloaded from TCGA. The data from TCGA used in this paper are publicly available for reasonable use.

Pan-cancer analysis. Univariate Cox regression (uniCox) and Kaplan-Meier analyses were conducted to explore the influence of FAM83A-AS1 on the survival of patients in pan-cancer using the R package 'survminer. (https://rpkgs.datanovia.com/survminer/index.html) and 'survival. (https://cran.r-project.org/web/packages/survival/). Overall survival (OS) was evaluated ($P<0.05$ was considered to indicate a statistically significant difference). Spearman's correlation analysis was used to evaluate the relationship between gene expression and TMB.

RNA extraction and reverse transcription-quantitative (RT-qPCR). The sequences of the primer sets were listed in Table SI. Total RNA from cells and fresh-frozen tissues were extracted using TRIzol reagent (Invitrogen; Thermo Fisher Scientific, Inc.) according to the manufacturer's protocol. cDNA was synthesized using the PrimeScript RT Reagent Kit (Takara Biotechnology Co., Ltd.). The reaction was carried out for 15 min at 37˚C, 5 min at 85˚C, and then 4˚C until further use. To quantitatively express the contents of RNA, RT-qPCR analysis was carried out using the SYBR Green Premix ExTaqTM kit (Takara Biotechnology Co., Ltd.) in the biological system 7500 sequence detection system (Applied Biosystems; Thermo Fisher Scientific, Inc.). Each reaction is performed three times. GAPDH, 18S, or U6 were used as the internal controls for microRNA and mRNA. The relative level of each target RNA was calculated using the $2^{-\Delta\Delta Cq}$ method (11).

Cell transfection. The 5-nmol small interfering (si)RNAs (Table SII) for FAM83A-AS1, miR-202 inhibitors, and si-negative control (si-NC) were obtained from Guangzhou RiboBio Co., Ltd. The sequence of si-FAM83A-AS1 and miR-202-3p inhibitor are listed in Table SII; however, the sequence of the corresponding control could not be provided due to confidentiality of the purchasing company. Lipofectamine iMAX (Thermo Fisher Scientific, Inc.) was used for transfection (si)RNAs in PC9 cells. FAM83A-AS1 was created by Invitrogen; Thermo Fisher Scientific, Inc. and then cloned into the pcDNA3.1 expression vector.and Lipofectamine 3000 (Thermo Fisher Scientific, Inc.) was used for transfection in A549 cells. The temperature and duration of transfection were according to the manufacturer's protocol. After transfecting for 24 h, PC9 and A549 cells were used for follow-up experiments.

Cell counting kit-8 (CCK-8). Using the CCK-8 assay, cell proliferation was evaluated (cat. no. C0038; Beyotime Institute of Biotechnology). CCK8 reagent was applied to each well for 1 h at 37˚C following 24, 48, or 72 h of siRNA and overexpression. Then, a microplate reader with an automated setting was used to measure the absorbance at 450 nm (BioTek Instruments, Inc.).

Table I. Clinicopathological characteristics of 399 patients included in the The Cancer Genome Atlas-lung adenocarcinoma dataset.

Clinicopathological characteristics	High risk no. (%)	Medium risk no. (%)	Low risk no. (%)	P-value
Age, years [mean (SD)]	65.1 (11.3)	65.4 (9.1)	66.8 (12.0)	0.858
Sex				0.704
Male	92 (46.7)	82 (42.5)	4 (44.4)	
Female	105 (53.3)	111 (57.5)	5 (55.6)	
T stage				0.456
T1	66 (33.5)	75 (38.9)	6 (66.7)	
T2	110 (55.8)	94 (48.7)	3 (33.3)	
T3	14 (7.1)	14 (7.3)	0 (0.0)	
T4	7 (3.6)	8 (4.1)	0 (0.0)	
Unknown	0 (0.0)	2 (1.0)	0 (0.0)	
N stage				0.038
N0	148 (75.1)	123 (64.1)	9 (100.0)	
N1	25 (12.7)	40 (20.8)	0 (0.0)	
N2	22 (11.2)	21 (10.9)	0 (0.0)	
Unknown	2 (1.0)	8 (4.2)	0 (0.0)	
M stage				0.921
M0	130 (66.3)	127 (66.8)	6 (66.7)	
M1	9 (4.6)	11 (5.8)	0 (0.0)	
Unknown	57 (29.1)	52 (27.4)	3 (33.3)	
Stage				0.089
I	129 (65.5)	106 (54.9)	9 (100.0)	
II	29 (14.7)	49 (25.4)	0 (0.0)	
III	26 (13.2)	24 (12.4)	0 (0.0)	
IV	9 (4.6)	11 (5.7)	0 (0.0)	
Unknown	4 (2.0)	3 (1.6)	0 (0.0)	
Smoke				0.004
Smoking	178 (92.2)	154 (79.8)	8 (88.9)	
Non-smoking	15 (7.6)	39 (20.2)	1 (11.1)	

Fluorescence-activated cell sorting (FACS). For apoptosis detection, the A549 and PC9 tumor cells were seeded into a 6-well plate and transfected after 24 h. Cells ($1x10^6$), both floating and adherent, were trypsinized and rinsed with PBS after the indicated treatments. Annexin V-FITC Apoptosis Detection kit I (BD Biosciences) was used to detect apoptotic cells by staining with Annexin V-FITC and PI according to the manufacturer's instructions at room temperature for 15 min. A flow cytometer (BD Biosciences) was used to access the early and late apoptosis of the cells.

5-Ethynyl-2'-deoxyuridine (EdU) assay. LUAD cells ($4x10^4$) were seeded into 96-well templates and harvested at 48 h post-transfection. Cells were then incubated with 50 mM EdU for 2 h at 37˚C, fixed with 4% paraformaldehyde and incubated with Apollo Dye Solution to label proliferating cells both 20-40 min at room temperature. Cell nuclei were counterstained by DAPI (1 μg/ml). Proliferating cells with green signals were visualized by a Leica DM4000 B LED fluorescent microscope.

Matrigel and Transwell assay. Cells ($4x10^4$) were sown in the upper Transwell assay chambers of 8-μm pore filters (for the migration assay). For the invasion assay, $4x10^4$ cells were seeded in serum-free media into the upper Matrigel assay chambers with a membrane coated (-20˚C) with Matrigel (Corning, Inc.). The medium in the lower chamber contained 10% FBS as chemokine. Non-migrating or non-invading cells were gently removed after incubation at 37˚C for 24 h for migration and 48 h for invasion. Cells that migrated to the bottom of the membrane were then fixed with 4% paraformaldehyde at room temperature for 30 min, stained with 0.5% crystal violet solution at room temperature for 30 min, and observed randomly under a fluorescent microscope at a magnification of x100.

Bioinformatics analysis. TargetScan (https://www.targetscan.org/vert_80/) and StarBase (https://starbase.sysu.edu.cn/starbase2/) database were used to predict RNA and potential interaction sites of RNA. miRanda database (ttp://www.microrna.org/microrna/home.do) was used to predict the

interaction sites of miRNA and mRNA. Kyoto Encyclopedia of Genes and Genomes pathway enrichment analysis was used to evaluate the degree of gene pathway enrichment.

RNA-binding protein immunoprecipitation (RIP). The Magna RIP kit was used to carry out a RIP assay (cat. no. 17-704; MilliporeSigma). An overnight incubation at 4˚C with 50 μl magnetic beads coated with antibodies against AGO2 (cat. no. 2897; Cell Signaling Technology, Inc.) or IgG (cat. no. 17-704; MilliporeSigma) was performed on a total of $1x10^7$ A549 or PC9 cells after they had been collected, lysed and incubated. The immunoprecipitated RNAs were purified, and quantified by RT-qPCR, and the beads were then washed with washing buffer.

Pull-down assay. Biotinylated FAM83A-AS1 probes and oligo probes (as negative controls) for the pull-down assay were created and manufactured by Shanghai GenePharma Co., Ltd. Streptavidin magnetic beads (Thermo Fisher Scientific, Inc.) were treated with biotinylated FAM83A-AS1 probes for 2 h at room temperature to create probe-coated magnetic beads. The microspheres were then treated with the cell lysate at 4˚C for an overnight period. Afterwards, the beads were washed. TRIzol® (Invitrogen; Thermo Fisher Scientific, Inc.) was used to extract the RNA and RT-qPCR was used to analyze it. The sequence of the FAM83A-AS1 probe was 5'-GGGCCTAAA CCGGTCGATTA-3' and the sequence of the oligo probe was 5'-ACACTTCTCGGATATACGCCCT-3'.

MiRNA pull down. By transfecting A549 and PC9 cells with 100 nM 3'-biotinylated miRNA mimics, a miRNA pull-down test was carried out. After the cells had been incubated at 37˚C for 24 h, they were twice rinsed with ice-cold PBS before being lysed with miRNA pull-down lysis buffer. Biotin-labeled miRNAs were extracted for the miRNA pull-down test by incubating the beads with 100 μl of cell lysate and 100 μl of the miRNA pull-down lysis buffer at 4˚C for 4 h while rotating the beads. The TRIzol® reagent was then used to isolate biotin-labeled miRNAs and the RNAs that interact with them. By using RT-qPCR, miRNA interacting RNAs were found.

Fluorescence in situ hybridization (FISH). After being fixed in 4% paraformaldehyde at room temperature for 10 min, A549 cells ($1x10^7$) were then rinsed with PBS. Afterwards, cells were permeabilized for 15 min at 4˚C using 0.5% Triton X-100 in precooled PBS. Cells were incubated for 4 h at 37˚C with a mixture of a Cy3-labeled FAM83A-AS1 probe, a Fam-labeled miR-202-3p targeting probe, and other substances included in the kit. According to the instructions, a FISH kit (Shanghai GenePharma Co., Ltd.) was used to find the probe signal. DAPI (1 μg/ml) was used to stain the nucleus. Images were captured with a TCS SP5II confocal microscope (Leica Microsystems GmbH).

Dual-luciferase reporter assay. TargetScan (http://www.targetscan.org) anticipated the 3' UTR binding sites of miR-202-3p and HK2 mRNA. The miR-202-3p seed sequence was altered (from TTCCATGTCCCTGTATAATTCTA to TAGGTACAGGGTGTATAATTCTA) and the wild-type (WT) and mutant (MUT) HK2 3'-UTR was introduced into the pGL3 basic vector to verify the binding specificity (Promega Corporation). Sequencing was used to confirm the validity of each vector, and the dual luciferase assay kit (cat. no. E1910; Promega Corporation) was used to measure luciferase activity. The relative luciferase activity was normalized to *Renilla* luciferase activity.

Western blot analysis. Western blot analyses were carried out according to standard protocols. For protein extract preparation, cells were lysed on ice with RIPA Lysis Buffer (Thermo Fisher Scientific, Inc.) containing complete protease and phosphatase inhibitor cocktail (Roche Diagnostics). Soluble protein extracts were separated by centrifugation at 13,000 g for 20 min. A bicinchoninic acid (BCA) Protein Assay kit was used for protein determination. The obtained cell lysates (20 μg protein per lane) were resolved on 4-20% sodium dodecyl-sulfate-polyacrylamide gel electrophoresis (SDS-PAGE) and transferred on polyvinylidene difluoride membraneHybond TM-P (Amersham Bioscience). Membranes were saturated with 5% bovine serum albumin (Thermo Fisher Scientific, Inc.) at room temperature for 2 h and incubated with the primary antibodies anti-HK2 (1:1,000; 2867S; Cell Signaling Technology, Inc.) at 4˚C overnight. Secondary anti-GAPDH (cat. no. 5174S; CST, Cell Signaling Technology, Inc.) all conjugated to Alexa Fluor 680 (Abcam) were incubated with the membranes for 2 h at room temperature at 1:10,000 dilution. All bands of western blot were detected and qualified with gray scale ratio by Odyssey CLx imaging systems (LI-COR Biosciences).

Extracellular flux assays. The extracellular flux analyzer Seahorse XF96e was used to quantify the extracellular acidification rate (ECAR) in cell lines (Agilent Technologies, Inc.). Following the manufacturer's instructions, glucose, oligomycin, and 2-Deoxy-D-glucose were sequentially added to the Seahorse Analyzer using the Glycolysis Stress Test kit (cat. no. 103020-100; Agilent Technologies Inc.) to measure the ECAR, which is used to evaluate important parameters of glycolytic flux (such as basal glycolysis and glycolytic capacity). Using a bicinchoninic acid (BCA) Protein Assay kit (cat. no. P0012; Beyotime, Institute of Biotechnology), all data were standardized to the protein concentrations.

D-Lactate assay. Intracellular lactate levels were measured using a D-Lactate Assay kit (cat. no. ab83429; Abcam) according to the manufacturer's instructions.

Statistical analysis. The statistical analysis was performed using GraphPad Prism 8.0 software (GraphPad Software, Inc.) and R version 4.1.2 software. R package 'Limma' was used to identify differentially expressed genes (DEGs) between different LUAD subtype. The false positive results using the default Benjamini-Hochberg false discovery rate (FDR) method. Survival analysis was based on the Kaplan-Meier method with a two-sided log-rank test. The majority of graphs display the mean and standard deviation as well as graphs for each data point. Paired Student's t-test was used to determine the significance, and the P-value was shown by an asterisk. One-way ANOVA test was used for data with multiple comparisons in data sets of three or more groups (e.g., Fig. 2A),

and an LSD post-hoc test was used. For Fig. 2E, a chi-square test was used to characterize the association of FAM83A-AS1 with the TN stage.

Results

Identification of high-risk pathological subtype-associated lncRNA, FAM83A-AS1. According to the annotation of H&E from TCGA-LUAD dataset, a total of 399 patients were included in the present study, composed of 9 patients in a low risk group, 193 patients in an intermediate risk group and 197 patients in the high-risk group. To identify the differentially expressed lncRNAs across the three histological pathology groups, transcriptional data of lncRNA were pairwise compared. Compared with the intermediate or high-risk group, there were 130 lncRNAs dysregulated in the low-risk group, consisting of 10 downregulated and 120 upregulated (|log2FC|>0.5, P<0.05, Table SIII). Compared with the low or high-risk group, there were 13 lncRNAs dysregulated in the intermediate-risk group, consisting of 3 downregulated and 10 upregulated (|log2FC|>0.5, P<0.05, Table SIV). Compared with the low and intermediate-risk group, there were 16 lncRNAs dysregulated in the high-risk group, consisting of 13 downregulated and 3 upregulated (|log2FC|>0.5, P<0.05, Table SV). Screening the differentially expressed lncRNAs between groups according to risk classification, it was found that FAM83A-AS1, CTD-2510F5.4, LINC00973 and KIFC1 were significantly upregulated in pathological subtypes ranging from low to high risk (Fig. 1B). the differentially expressed lncRNAs between the LUAD tumor tissues and the adjacent normal tissues in the TCGA-LUAD dataset were also characterized, and the differential expression of FAM83A-AS1 ranked the top (Fig. 1C). Univariate regression analysis was performed, which revealed that FAM83A-AS1 was associated with a poorer prognosis and a higher risk of recurrence (Fig. 1D).

It was also identified that the expression of FAM83A-AS1 increased gradually from the low-risk group to the high-risk group (Fig. 2A). Concurrently, it was also significantly increasingly expressed in higher N-stage and T-stage (Fig. 2B and C). The mRNA expression levels were also analyzed using PCR in our paired adenocarcinoma tissues with clinical stage data and differentiated low and high based on the median expression level of FAM83A-AS1, which confirmed that FAM83A-AS1 is highly expressed in tumors as well as in higher clinical stages (Fig. 2D and E). Collectively, these data revealed that FAM83A-AS1 was upregulated in tumor tissues compared with normal tissues, particularly in patients with high-risk pathological subtypes and higher clinical stages.

Pan-cancer analysis of FAM83A-AS1. Next, features of FAM83A-AS1 were characterized through pan-cancer analysis. Pan-cancer analysis showed that FAM83A-AS1 was upregulated in multiple cancers, particularly in LUAD (Fig. 3A). Spearman's correlation analysis revealed that high expression of FAM83A-AS1 was significantly associated with high TMB both in Thymoma (THYM) and LUAD (Fig. 3B). Concurrently, FAM83A-AS1 was revealed to be a potential risk factor for tumor patients in most cancers (Fig. 3C). In LUAD, Kaplan-Meier survival curves indicated that patients with high FAM83A-AS1 expression had significantly worse OS than patients with low expression (Fig. 3D). The DNA methylation level of the FAM83A-AS1 promoter region was also explored. The average distribution of the beta values of the methylation probes cg0831735 and cg054279078 located in the FAM83A-AS1 promoter region was not significantly different between tumor and normal tissue, and they were both located in the fully methylated region (beta >0.6); however, in the partially methylated region [beta in (0.2, 0.6)], the distribution in tumor tissue was significantly more than that in normal tissue (Fig. 3E). Methylation levels are negatively correlated with gene expression in most cases. Therefore, the methylation differences of FAM83-AS1 promoter region between tumor and normal tissues in LUAD may be a possible epi-regulatory mechanism leading to its upregulated expression of FAM83A-AS1 in tumors. Collectively, the pan-cancer analysis revealed that increased expression level of FAM83A-AS1 was positively correlated with the poor prognosis of patients and was also significantly associated with high TMB in LUAD, which may be caused by the dysregulated methylation of the promoter region of FAM83A-AS1.

FAM83A-AS1 promotes malignancy of LUAD in vitro. The role of FAM83A-AS1 in LUAD malignant progression was further validated through functional assays. Firstly, the endogenous expression of FAM83A-AS1 in LUAD cell lines was investigated using RT-qPCR, which revealed that the endogenous expression of FAM83A-AS1 was higher in all cancer cell lines than that of normal lung epithelial cell lines HBE, and the expression of FAM83A-AS1 was relatively higher in PC9 cell lines while it was relatively lower in A549 cell lines (Fig. 4A), both of which were selected for the next experimental assays. A total of three pairs of siRNAs were designed to decrease the expression of FAM83A-AS1 (si-FAM83A-AS1-1, si-FAM83A-AS1-2 and si-FAM83A-AS1-3), which were transfected into the PC9 cell line. The RT-qPCR results revealed that si-FAM83A-AS1-2 was the most efficient siRNA in FAM83A-AS1 knockdown (Fig. 4B), which was selected to inhibit FAM83A-AS1 expression. In addition, A549 cell lines were transfected with the plasmid of mock or FAM83A-AS1, which revealed that overexpression of FAM83A-AS1 significantly increases FAM83A-AS1 expression (Fig. 4C). Transwell migration and Matrigel invasion assays revealed that overexpressing FAM83A-AS1 significantly promoted the migration and invasion of LUAD cell lines (Fig. 4D). While CCK-8 and EdU assays were performed to identify that overexpression of FAM83A-AS1 efficiently facilitates cell growth in A549 cells (Fig. 4E and H). Overexpression of FAM83A-AS1 also reduced cell apoptosis (Fig. 4I). By contrast, the knockdown of FAM83A-AS1 significantly suppressed migration, invasion, and growth and induced apoptosis of LUAD cell lines (Fig. 4F and G). Taken together, the aforementioned data indicated that FAM83-AS1 is functionally important in promoting the malignancy of LUAD.

FAM83A-AS1 acts as a sponge to interact with miR-202-3p. Next, the potential biological mechanism of FAM83A-AS1 was explored. LncRNAs are known to play numerous important roles, one of which is acting as miRNA sponges (12). To explore the miRNA absorption capacity of FAM83H-AS1, a

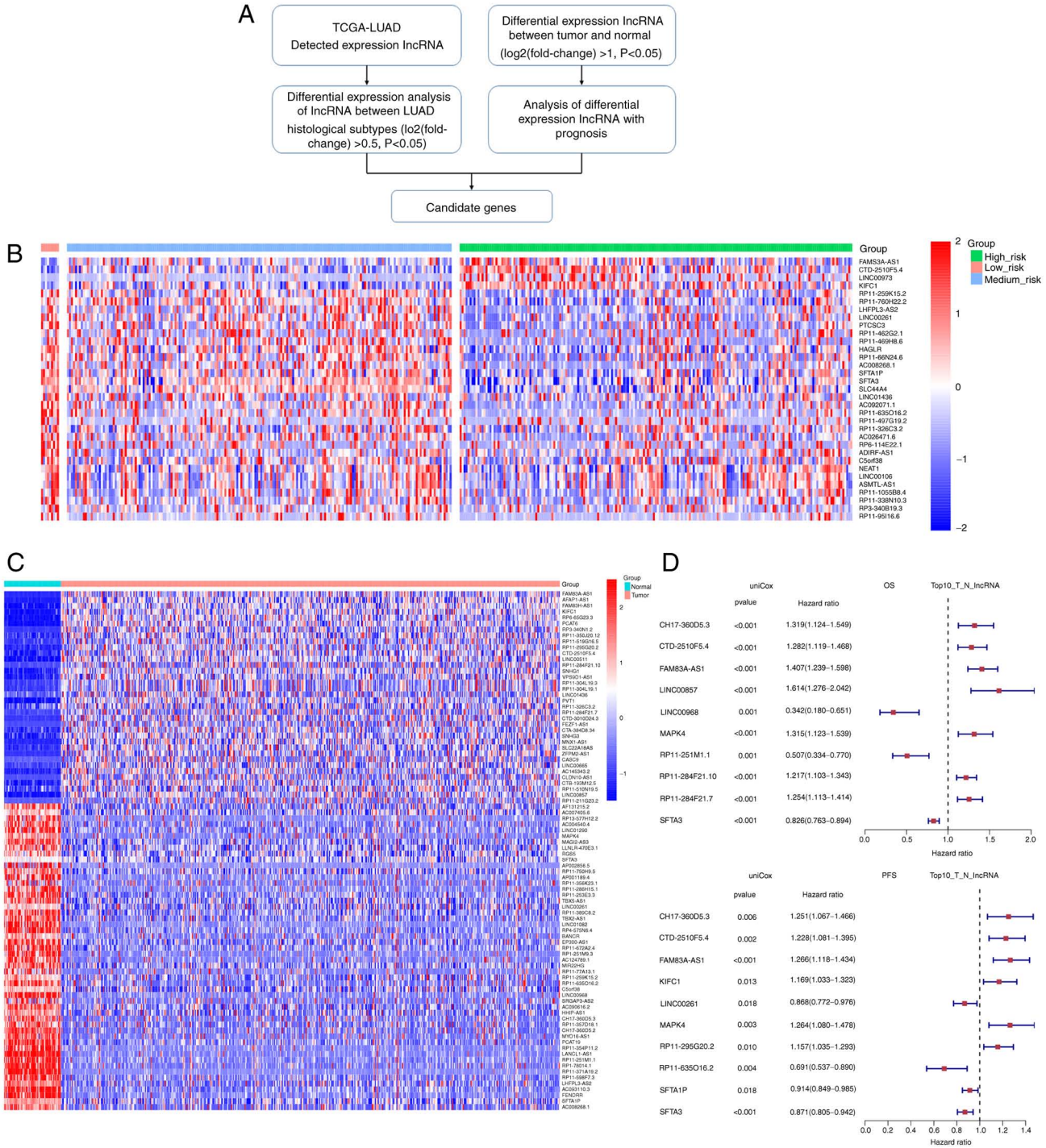

Figure 1. Identification of high-risk pathological subtype-associated lncRNA, FAM83A-AS1. (A) Screening of lncRNAs that differentially expressed between the three histological pathology risk groups, and between tumor tissues and adjacent normal tissues of LUAD. (B) Heatmap of lncRNAs in pathological subtypes ranging from low to high risk. (C) Heatmap of lncRNAs between the LUAD tumor tissues and the adjacent normal tissues in the cancer genome atlas (TCGA-LUAD) dataset. (D) Univariate regression analysis of top 10 lncRNAs between tumor tissues and adjacent normal tissues of LUAD in OS and PFS. lncRNA, long non-coding RNA; LUAD, lung adenocarcinoma; OS, overall survival; PFS, progression-free survival.

RIP experiment of Ago2 was conducted both in A549 and PC9 cells. The results demonstrated that FAM83H-AS1 was significantly enriched by an anti-Ago2 antibody compared with IgG (Fig. 5A), which indicated that the biological function of FAM83A-AS1 may be through miRNA sponging (13). The potential miRNAs that interacted with FAM83A-AS1 were further identified through bioinformatics analysis of two databases, TargetScan and StarBase (14). After screening the potential sponged miRNAs, miR-202-3p was selected, the seed sequences of which are partially complementary to FAM83A-AS1 (Fig. 5B). To confirm the interaction between FAM83A-AS1 and miR-202, FAM83A-AS1 and miR-202 mRNA expression was examined in patients with LUAD in TCGA database and it was observed that miR-202 negatively correlated with FAM83A-AS1 expression (R=-0.13, P=0.0025) (Fig. 5C). To verify whether this candidate miRNA could

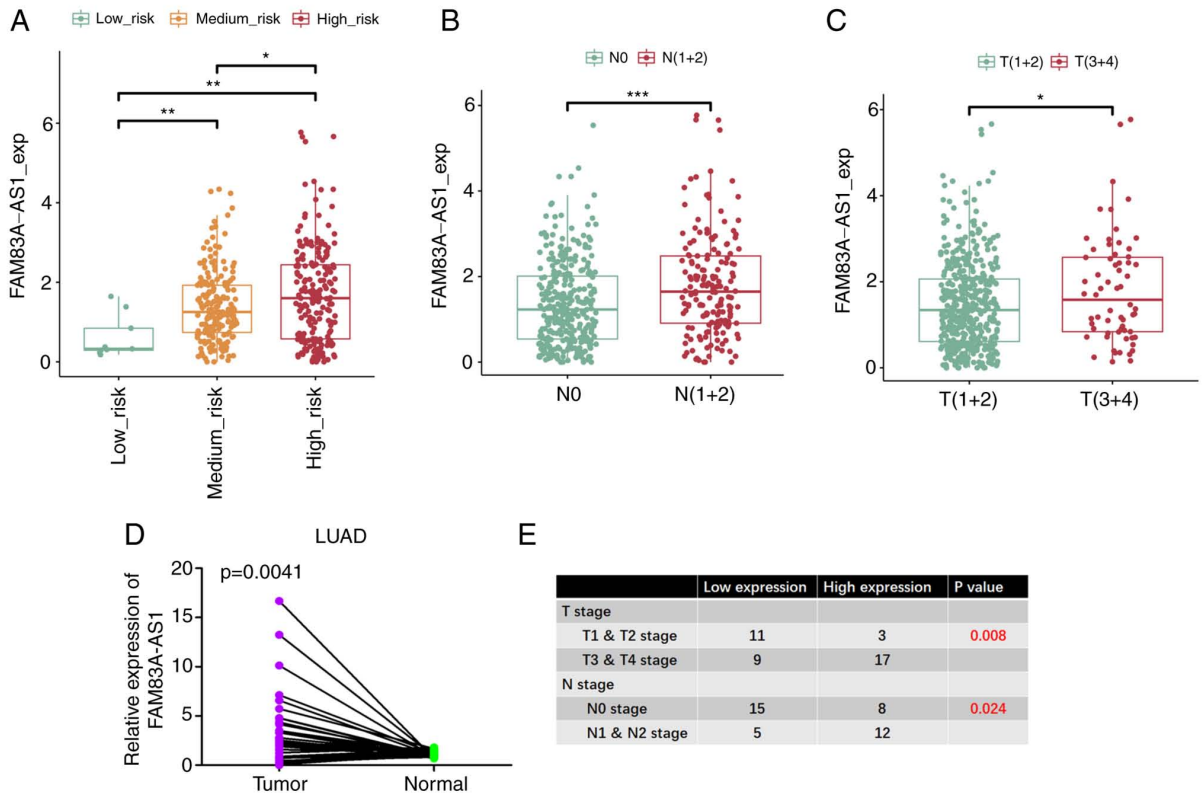

	Low expression	High expression	P value
T stage			
T1 & T2 stage	11	3	0.008
T3 & T4 stage	9	17	
N stage			
N0 stage	15	8	0.024
N1 & N2 stage	5	12	

Figure 2. FAM83A-AS1 is highly expressed in tumor tissues and patients with high-risk pathological subtypes and higher clinical stages. (A) Different expression of FAM83A-AS1 from low-risk group to high-risk group. (B) Different expression of FAM83A-AS1 between N0-stage and N (I + II)-stage. (C) Different expression of FAM83A-AS1 between T (I + II)-stage and T (III + IV)-stage. (D) The relative expression levels of FAM83A-AS1 in LUAD tissues and the adjacent non-cancerous tissues were determined by reverse transcription-quantitative PCR. (E) Tumor clinical stages of patients in low expression and high expression cohort. LUAD, lung adenocarcinoma. *P<0.05, **P<0.01 and ***P<0.001 (Student's t-test).

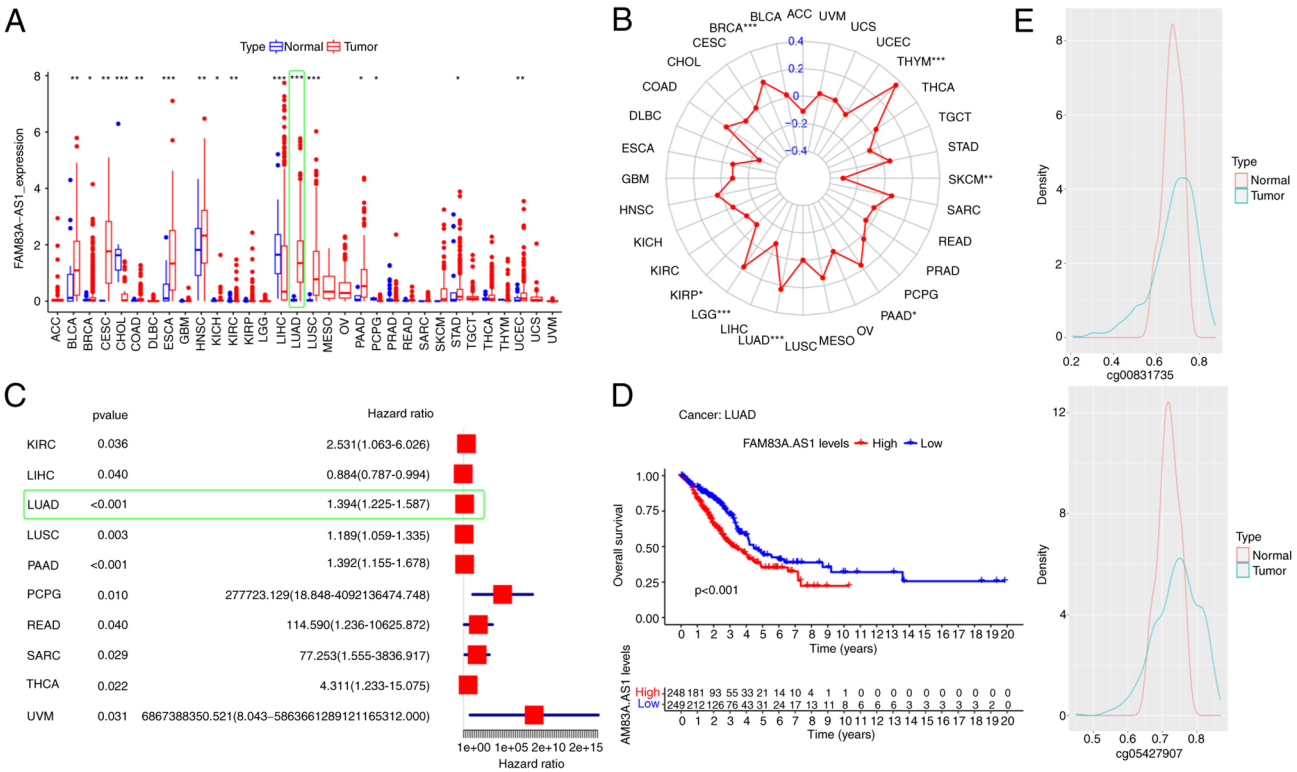

Figure 3. Pan-cancer analysis of FAM83A-AS1. (A) Pan-cancer analysis of FAM83A-AS1 expression in multiple cancers. (B) Spearman correlation analysis between FAM83A-AS1 and tumor mutational burden in different cancer types. (C) Nomogram of FAM83A-AS1 in various cancers. (D) Kaplan-Meier analysis of overall survival in LUAD according to FAM83A-AS1 expression level. (E) DNA methylation level of the FAM83A-AS1 promoter region in tumor and normal tissue by methylation probes. *P<0.05, **P<0.01 and ***P<0.001 (Student's t-test). LUAD, lung adenocarcinoma.

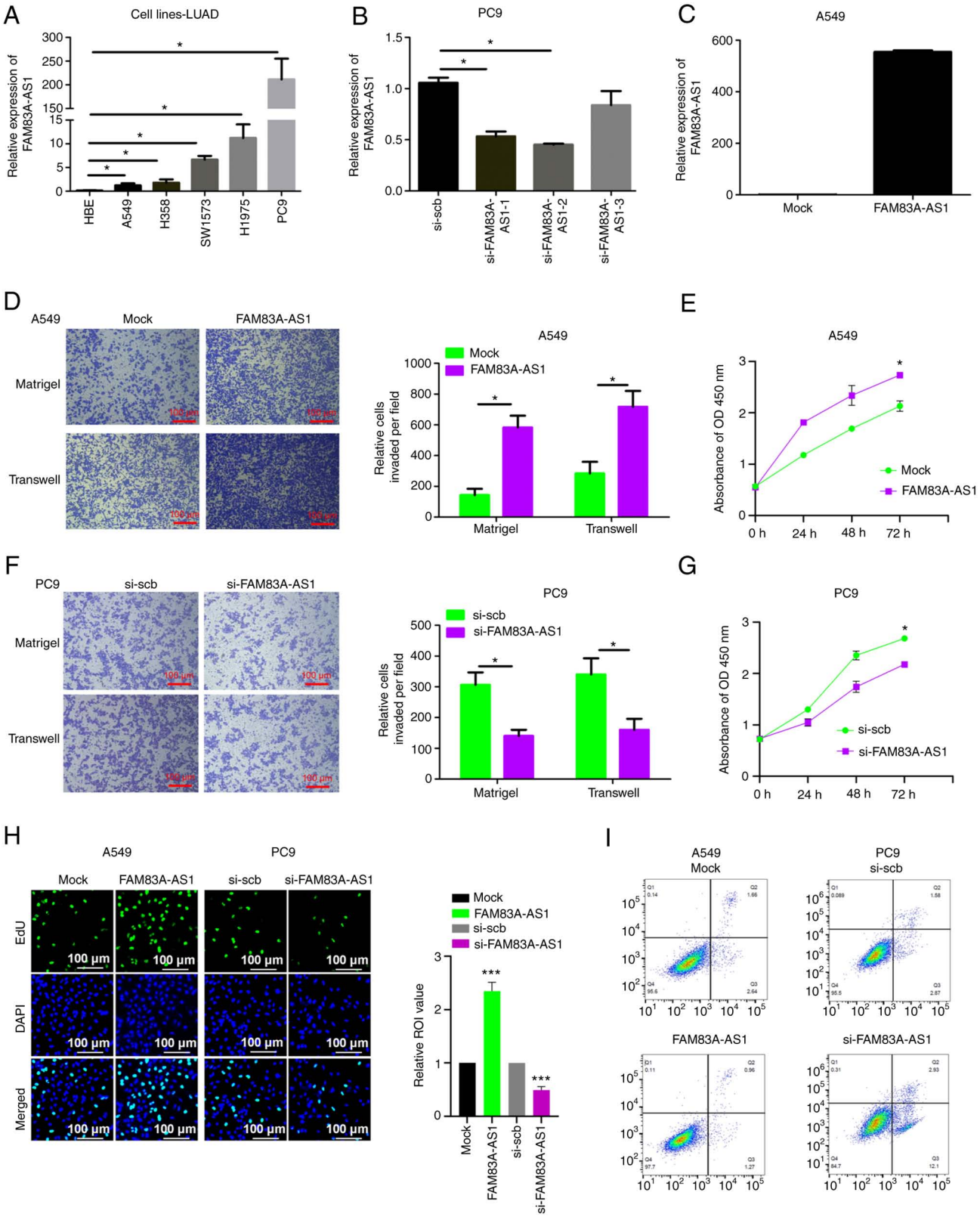

Figure 4. FAM83A-AS1 promotes malignancy of LUAD *in vitro*. (A) FAM83A-AS1 expression levels in LUAD cell lines (A549, H358 SW1573 H1975 and PC9) and a normal lung cell line (HBE). (B and C) Validation of the knockdown (B) and overexpression (C) efficacy of FAM83A-AS1 in PC9 and A549 cell lines by reverse transcription-quantitative PCR, si-scramble (si-scb) and Mock as a negative control. (D) Representative images and bar graphs depicting the migration and invasion abilities of FAM83A-AS1 overexpressing A549 cells by Transwell migration and Matrigel invasion assays. (E) Effects of FAM83A-AS1-overexpressing A549 cells in cell proliferation measured by CCK-8 assays. (F) Representative images and bar graphs depicting the migration and invasion abilities of FAM83A-AS1-knockdown PC9 cells by Transwell migration and Matrigel invasion assays. (G) Effects of FAM83A-AS1-knockdown PC9 cells proliferation measured by CCK-8 assays. (H) Representative images and bar graphs depicting the cell proliferation of FAM83A-AS1 knockdown and overexpression in PC9 and A549 cell lines by 5-Ethynyl-2'-deoxyuridine assay. (I) Fluorescence activated Cell Sorting analysis of the effects of FAM83A-AS1 on apoptosis in FAM83A-AS1 overexpressing A549 cells and FAM83A-AS1-knockdown PC9 cells. All the results are presented as the mean ± SD (n=3), which were three separate experiments performed in triplicate. *P<0.05 and ***P<0.001 (Student's t-test). LUAD, lung adenocarcinoma; si-, small interfering; CCK-8, Cell Counting Kit-8.

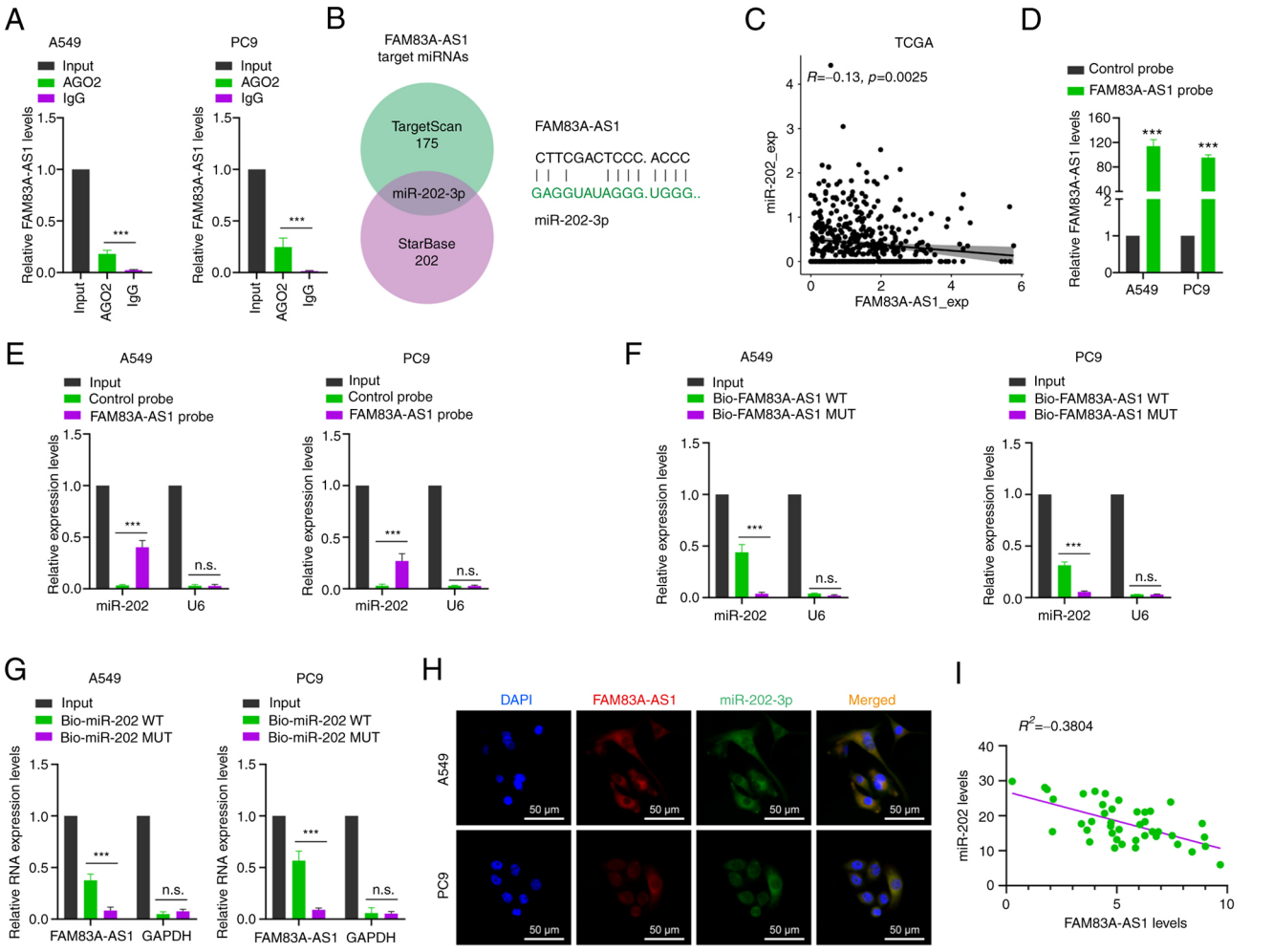

Figure 5. FAM83A-AS1 acts as a sponge to interact with miR-202-3p. (A) RNA Binding Protein Immunoprecipitation assay was performed using an Ago2 antibody, and IgG served as a negative control. (B) The Venn diagram shows the intersection of miRNA lists. (C) FAM83A-AS1 mRNA and miR-202-3p expression was analyzed in patients with LUAD in TCGA. (D) RT-qPCR results showed that FAM83A-AS1 could be specifically enriched by FAM83A-AS1 probe. (E) The relative expression levels of FAM83H-AS1 were detected by RT-qPCR in A549 and PC9 cell lysates using the control probe or FAM83H-AS1 probe. (F) The expression levels of miR-202-3p and small nuclear RNA U6 were detected by RT-qPCR in A549 and PC9 cell lysates using WT Bio-FAM83H-AS1 probe or MUT Bio-FAM83H-AS1 probe. (G) FAM83A-AS1 was enriched by biotinylated WT or MUT-miR-202-3p, and RT-qPCR was used to determine the relative FAM83A-AS1 mRNA levels. (H) RNA fluorescence in situ hybridization images showed the localization of FAM83A-AS1 and miR-202-3p in A549 cells (scale bar, 50 μm). (I) Expression of FAM83A-AS1 and miR-202-3p was measured using RT-qPCR in LUAD tissues. All the results are presented as the mean ± SD (n=3), which were three separate experiments performed in triplicate. ***P<0.001 (Student's t-test). LUAD, lung adenocarcinoma; miRNA or miR, microRNA; TCGA, The Cancer Genome Atlas; RT-qPCR, reverse transcription-quantitative PCR; WT, wild-type; MUT, mutant; n.s., no significance.

directly bind to LncFAM83H-AS1, the lncRNA pull-down experiment was conducted using the FAM83H-AS1 probe labeled with biotin. As expected, the biotin probe bonded specifically to FAM83H-AS1 (Fig. 5D). In both A549 and PC9 cell lines, miR-202-3p was significantly enriched by the lncFAM83H-AS1 probe compared with the control probe (Fig. 5E). To further confirm the interaction between FAM83A-AS1 and miR-202-3p, the MUT biotinylated probes of FAM83A-AS1 and miR-202-3p were designed, respectively, according to the complementary sequences. Compared with the wide-type probe of FAM83A-AS1, the MUT probe of FAM83A-AS1 could not significantly enrich miR-202-3p both in A549 and PC9 cell lines (Fig. 5F). A biotinylated miR-202-3p pull-down experiment was also conducted and the results revealed that the enrichment of FAM83H-AS1 by the MUT miR-202-3p probe was significantly reduced compared with the WT miR-202-3p probe (Fig. 5G). In addition, FISH analysis revealed co-localization of miR-202-3p and lncFAM83H-AS1 in the cytoplasm (Fig. 5H). A significant negative correlation was also found between FAM83H-AS1 and miR-202-3p in LUAD tissues (R2=-0.3804, P<0.001) (Fig. 5I). Collectively, these results suggested that FAM83H-AS1 acts as a sponge to directly bind miR-202-3p.

FAM83A-AS1 regulates miR-202-3p/HK2 axis to mediate glycolysis. Previous studies have found that lncRNA may play an important role in tumor progression through the lncRNA-miRNA-mRNA signaling pathway (15). To explore the downstream target of FAM83A-AS1, the co-expression pattern of FAM83A-AS1 and mRNAs was first analyzed according to the expression data from TCGA. Kyoto Encyclopedia of Genes and Genomes pathway enrichment analysis showed that FAM83A-AS1 was significantly enriched in central carbon metabolism, glycolysis and mannose type O-glycan biosynthesis (Fig. 6A, upper). The potential target genes of miR-202-3p were also predicted by the intersection of miRanda

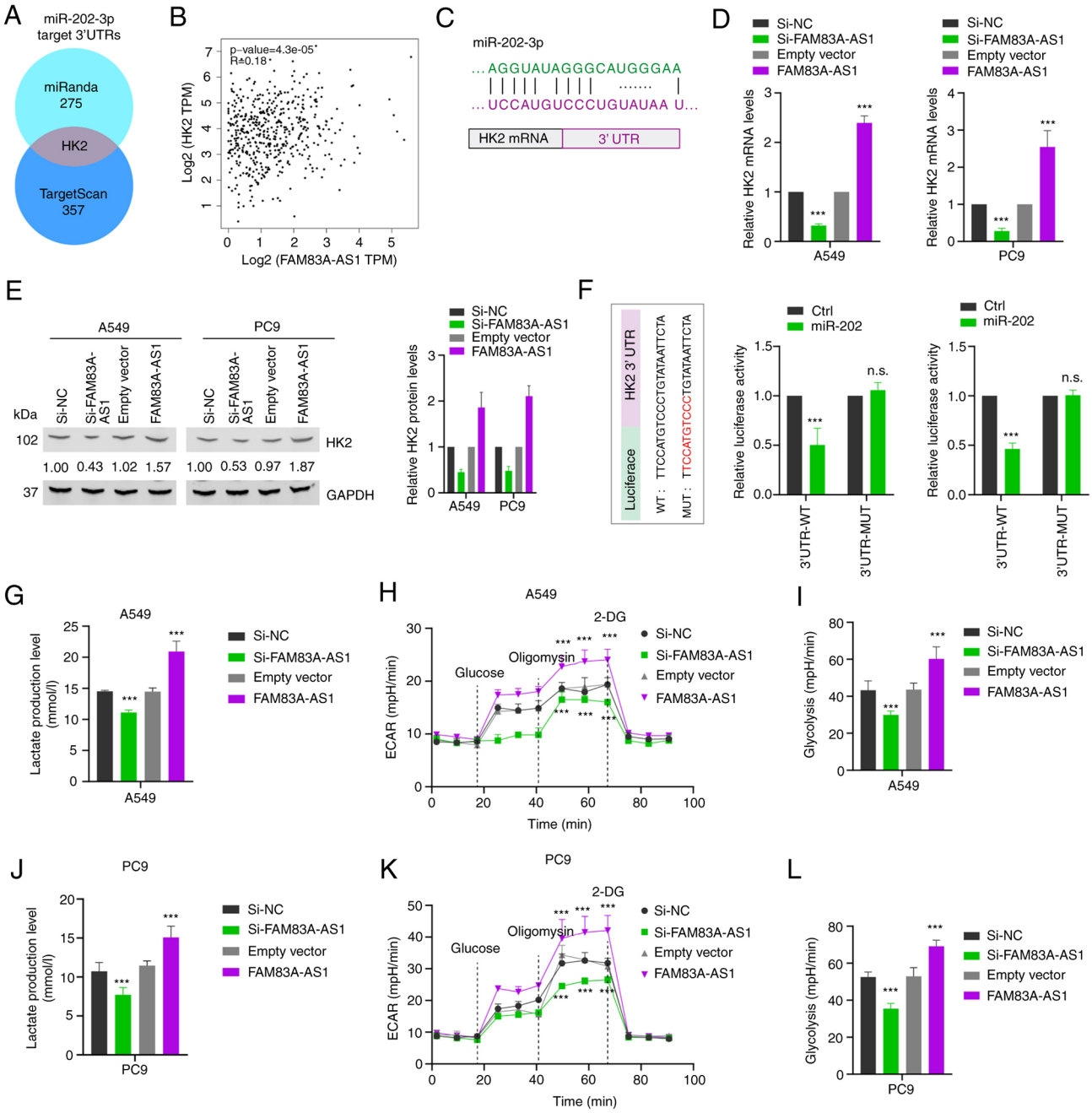

Figure 6. FAM83A-AS1 regulates miR-202-3p/HK2 axis to mediate glycolysis. (A) Left: Kyoto Encyclopedia of Genes and Genomes enrichment analysis showed the revealed signaling pathways associated with FAM83A-AS1. Right: The Venn diagram shows overlapping the FAM83A-AS1 associated genes referred to glycolysis and the potential target genes of miR-202-3p by miRanda. (B) Expression of FAM83A-AS1 and HK2 in The Cancer Genome Atlas database. (C) MiR-202-3p can bind to the 3'-UTR of HK2 mRNA. (D) The mRNA level of HK2 in A549 and PC9 cells after knockdown or overexpression of FAM83A-AS1 was determined by reverse transcription-quantitative PCR, random oligo as a NC. (E) The expression levels of HK2 protein in A549 and PC9 cells with knockdown or overexpression of FAM83A-AS1 were detected by western blot analysis. (F) Left: Schematic graph illustrated the WT and mutation MUT of potential binding site between miR-202-3p and the 3'-UTR regions of HK2. Right: The direct binding between HK2 3'-UTR and miR-202-3p was analyzed by dual-luciferase reporter assay. (G and J) Lactic acid levels were detected after FAM83A-AS1 knockdown or overexpression in A549 and PC9 cells. (H and I, K and L) ECAR and glycolysis levels were detected after FAM83A-AS1 knockdown or overexpression in (H and I) A549 and (K and L) PC9 cells; 2-DG is a glucose analogue. All the results are presented as the mean ± SD (n=3), which were three separate experiments performed in triplicate. ***P<0.001 (Student's t-test). HK2, hexokinase II; miR, microRNA; UTR, untranslated region; NC, negative control; WT, wild-type; MUT, mutant; ECAR, extracellular acidification rate; 2-DG, 2-Deoxy-D-glucose; n.s., no significance.

(Table SVI). Overlapping the FAM83A-AS1-associated genes referred to glycolysis (Table SVII) and the potential target genes of miR-202-3p (Fig. 6A, lower), focus was addressed on the HK2 mRNA: i) There was a positive correlation between FAM83A-AS1 and HK2 transcriptional expression in TCGA database (Fig. 6B). ii) The 3'UTR of HK2 harbored sequences complementary to miR-202-3p sequences (Fig. 6C). iii) RT-qPCR and western blot analysis were used to detect the transcription and protein level of HK2, respectively, when cells were transfected with knockdown or overexpression of FAM83A-AS1 in A549 and PC9 cell lines. The results revealed that overexpressing FAM83A-AS1

increased the expression level of HK2 both in transcription and protein levels, while decreasing FAM83A-AS1 suppressed the expression level of HK2 (Fig. 6D and E). Subsequently, the dual-luciferase reporter assay showed that the luciferase activity was significantly reduced after co-transfection of miR-202-3p and HK2 3' UTR WT reporter plasmid, but not by MUT HK2 plasmid (Fig. 6F). HK2 has been reported to promote aerobic glycolysis of tumor cells (16). Therefore, lactate levels were measured, which showed that overexpression of FAM83A-AS1 significantly increased tumor cell lactate level while knockdown of FAM83A-AS1 significantly reduced the lactate level (Fig. 6G and J). Additionally, the Seahorse XF24e Extracellular Flux Analyzer was utilized to detect the ECAR of LUAD cells, referred to as glycolysis. It was demonstrated that FAM83A-AS1 knockdown significantly impaired glycolysis in A549 (Fig. 6H and I) and PC9 cell lines (Fig. 6K and L), which was consistent with the reduced level of lactate production. Collectively, these data indicated that FAM83A-AS1 sponges miR-202-3p to regulate the expression of HK2, which medicates cancer metabolic reprogramming.

FAM83A-AS1 promotes the malignant progression of LUAD depending on miR-202-3p. To further confirm the biological function of FAM83A-AS1 dependent on miR-202-3p, FAM83A-AS1 siRNA and miR-202-3p inhibitor were co-transfected into A549 and PC9 cell lines. CCK-8 and Transwell experiments revealed that knockdown of lncFAM83H-AS1 successfully inhibited cell proliferation and migration, while co-transfection of miR-202-3p inhibitor reversed the inhibition by FAM83A-AS1 (Fig. 7A and B). Additionally, it was explored whether the regulatory relationship between FAM83A-AS1 and HK2 is dependent on miR-202-3p. HK2 mRNA expression levels were decreased both in A549 and PC9 cell lines when transfected with the knockdown of FAM83A-AS1, while they were rescued when miR-202-3p inhibitors were co-transfected (Fig. 7C and D). Finally, a decreased glycolysis level was observed when the expression level of FAM83-AS1 was inhibited, which was consistent with the previous data. While co-transfection of FAM83A-AS1 and miR-202-3p inhibitors could partly rescue the glycolysis level of A549 and PC9 cell lines (Fig. 7E-J). These results suggested that LncFAM83H-AS1 promotes the malignant progression and glycolysis of LUAD depending on miR-202-3p.

Discussion

In the present study, the differential expressed lncRNAs across the three different histological pathology risk groups were explored, and FAM83A-AS1 was selected as the candidate lncRNA, which was positively associated with high-risk histological subtypes and higher clinical stages. Pan-cancer analysis revealed that FAM83A-AS1 was positively correlated with high TMB and poor prognosis in LUAD. The increased expression of FAM83A-AS1 may result from the hypomethylation of the promoter region. It was also revealed that FAM83A-AS1 promoted the progression of LUAD cancer cell lines *in vitro*. Additionally, FAM83A-AS1 functioned as a ceRNA to sponge miR-202-3p to upregulate the expression of HK2, which facilitated the malignant progression and glycolysis (16).

The aforementioned study mainly focused on the genomic diversity in the potential molecular mechanisms that determine the individual histological subtype of LUAD. Caso *et al* (17) employed targeted next-generation sequencing (NGS), and revealed that tumors in the high-risk group had higher copy number amplifications, as well as statistical significance alteration in three oncogenic pathways (p53, Wnt, Myc), compared with those in the intermediate or low-risk group. Whole-genome sequencing of tumor cell clusters from MIP in breast cancer shares high-frequency copy-number loss of PRDM16 and IGSF9 and the copy-number gain of ALDH2 (18). In addition to the genomic instability, non-genetic factors also contributed to the functional and phenotypic heterogeneity of histological pathology. Integrating with molecular data from >2,000 LUAD patients, Tavernari *et al* (19) identified that epigenetic and transcriptional reprogramming reshaped cancer cell identity to decipher the transition of histological pathology from indolent to aggressive patterns. In addition, the tumor microenvironment also contributed to the determination of the individual histological subtypes. It has been demonstrated that paracrine TGF-β signaling activation secreted by cancer-associated fibroblasts induced a solid-to acinar transition in lung cancer cells (20). In the current study, focus was addressed on the important members of transcriptome RNA, lncRNAs, and the increased expression of FAM83A-AS1 was identified; it showed a positive correlation with high-risk histological subtype group and higher clinical stages. It was also revealed that FAM83A-AS1 promoted migration, invasion and growth of LUAD cancer cells, which was positively associated with poorer prognosis.

Certain studies have been reported to explore the potential molecular mechanisms that determine the individual histological subtype of LUAD. Utilizing NGS, the genomic diversity of different histologic subtypes has been revealed (17). Compared with the intermediate or low-risk group, patients in the high-risk group had higher TMB, a rate of whole genome doubling, and several oncogenic pathways altered. Tumors with a higher percentage of MIP tended to harbor more chromosome instability, as well as the alteration in cyclin-dependent kinase inhibitor 2A, mammalian target of rapamycin, transcription termination factor 1 and brain-specific angiogenesis inhibitor 3 (21). In addition to the genomic mutation spectrum of lung cancer cells, transcriptomic features have also been reported to be associated with the histologic phenotype of lung cancer (22,23). However, as one of the important members of transcriptome RNA, little is known about the roles of lncRNA in the molecular features of LUAD histologic patterns.

LncRNAs play an important role in regulating the human genome due to their specific functions in various physiological and pathological processes (6). LncRNA FAM83A-AS1, which has been suggested to promote the development of tumors, is transcribed from the antisense strand of the FAM83A gene located at 8q24.13 (24). An increasing number of studies have reported that lncRNA-FAM83A-AS1 has potential carcinogenic ability in esophageal cell squamous carcinoma (25) HCC (26), and particularly LUAD. Wang *et al* (27) determined that FAM83A-AS1 increased FAM83A expression by enhancing FAM83A pre-mRNA stability and promoted the tumorigenesis of LUAD. One of the main mechanisms that lncRNA modulates gene expression is its interaction with

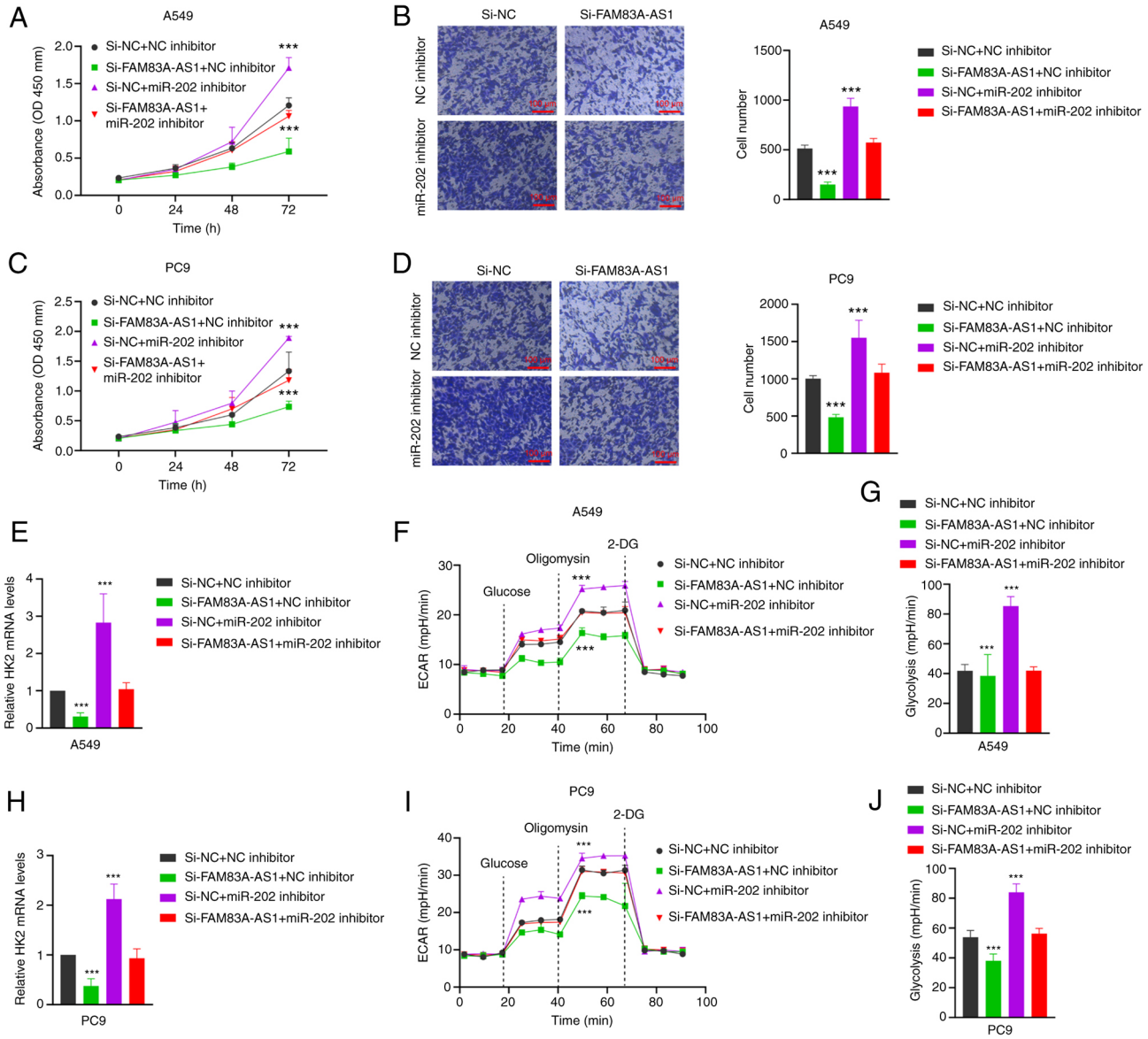

Figure 7. FAM83A-AS1 promotes the malignant progression of LUAD depending on miR-202-3p. (A-D) Cell Counting Kit-8 and Transwell assays were performed in A549 and PC9 cells after FAM83A-AS1 knockdown or FAM83A-AS1 siRNA and miR-202-3p inhibitor were co-transfected, random oligo was used as a NC. (E and H) The expression level of HK2 in A549 and PC9 cells were analyzed by reverse transcription-quantitative PCR after FAM83A-AS1 knockdown or FAM83A-AS1 siRNA and miR-202-3p inhibitor were co-transfected. (F and G, I and J) ECAR and glycolysis levels were detected after FAM83A-AS1 knockdown or FAM83A-AS1 siRNA and miR-202-3p inhibitor were co-transfected in (F and G) A549 and (I and J) PC9 cells; 2-DG is a glucose analogue. All the results are presented as the mean ± SD (n=3), which were three separate experiments performed in triplicate. ***P<0.001 (Student's t-test). si-, small interfering; miR, microRNA; NC, negative control; HK2, hexokinase II; ECAR, extracellular acidification rate; 2-DG, 2-Deoxy-D-glucose.

miRNA as a ceRNA to prevent miRNA from binding to the target RNA, including FAM83A-AS1 (14). For example, Xiao *et al* (28) identified that FAM83A-AS1 promotes LUAD cell migration and invasion by targeting miR-150-5p and modifying MMP14. In addition, there are several studies explaining the ceRNA mechanism between FAM83A-AS1 and miR-141-3p (13) or miR-214 (25). In the present study, a ceRNA model involving FAM83A-AS1, miR-202-3p and HK2 in LUAD was proposed. The potential miRNAs that interacted with FAM83A-AS1 were identified through bioinformatics analysis of two databases, TargetScan and StarBase, and miR-202-3p was finally selected. At the same time, it was found that overexpressing FAM83A-AS1 increased the expression level of HK2 both in transcription and protein levels, while decreasing FAM83A-AS1 suppressed the expression level of HK2. In summary, these findings support the authors' hypothesis and reveal a novel ceRNA regulatory axis (FAM83A-AS1-miR-203-3p-HK2) in LUAD cells.

The abnormal metabolism of tumor cells is considered one of the hallmarks of cancer, while glycolysis is regarded as the main way of energy metabolism in the tumor (29). Glycolysis is closely correlated with the tumor malignant degree. The rate-limiting enzyme HK2 in the glycolytic pathway plays an important role in the regulation of aerobic glycolysis (30). For example, Tantai *et al* (31) reported that TRIM46 activates AKT/HK2 signaling by modifying PHLPP2 ubiquitylation to promote glycolysis of lung cancer cells. Except the AMPK, the PI3K/Akt pathway, HIF-1α, and c-Myc, increasing

evidence showed that non-coding RNAs, including lncRNAs, participate in glycolysis by regulating HK2 gene expression in different types of cancer (32). Chen *et al* (33) stated that lncRNA PVT1 modulates HK2 expression by competitively binding to miR-143 to regulate aerobic glucose metabolism in gallbladder cancer. Yu *et al* (34) reported that MIR210HG regulates glycolysis, cell proliferation, and metastasis of pancreatic cancer cells through miR-125b-5p/HK2/PKM2 axis. In the present study, it was found that overexpressing FAM83A-AS1 increased the expression level of HK2 both in transcription and protein levels through sponging miR-202-3p. Meanwhile, overexpression of FAM83A-AS1 significantly increased tumor cell lactate levels. Moreover, FAM83A-AS1 knockdown significantly impaired glycolysis by detecting the ECAR of LUAD cells, suggesting that FAM83A-AS1 promotes LUAD cell glycolysis. It was revealed that FAM83A-AS1 sponged miR-202-3p to regulate the expression of HK2 in post-transcription, which facilitated the malignancy and glycolysis. The present study, to the best of our knowledge, is the first to document and interlink the FAM83A-AS1/miR-202-3p/HK2 axis in regulating malignancy and glycolysis of LUAD, which provided a novel avenue to addressing the determination of histologic patterns. In the present study, focus was addressed on the function and the mechanism of FAM83A-AS1 in the intrinsic characteristics of the tumor. However, it is unknown whether FAM83A-AS1 is expressed in other cell types in the tumor microenvironment such as macrophages, and $CD8^+$ T cells also, which may have a distinct function and mechanism, all of which should be explored further both *in vivo* and *in vitro*.

In conclusion, it was identified that FAM83A-AS1 was positively associated with high-risk pathological subtype and higher clinical stages, and it functioned as a ceRNA to sponge miR-202-3p to regulate the HK2 expression at post-transcription, which promotes the malignancy and glycolysis of LUAD.

Acknowledgements

Not applicable.

Funding

The present study was supported by The Jiangsu Province 'Six Talent Peaks Project' (grant no. WSN-027).

Availability of data and materials

All data generated or analyzed during this study are included in this published article.

Authors' contributions

XX and LZ contributed to sample and data acquisition and manuscript drafting. XX, LZ, BZ and DX offered technical support. XX, LZ, CC, GD and WX made substantial contributions to the conception and design of the study, funding of the study, and supervision. GD and WX confirm the authenticity of all the raw data. All authors were involved in writing the paper and read and approved the final version of the manuscript.

Ethics approval and consent to participate

The present study was approved (approval no. IACUC-2017088-1) by the Ethics Committee of the The First Affiliated Hospital of Nanjing Medical University (Nanjing, China) and complied with the ethical standards of the institution. Written informed consent was provided by all enrolled participants.

Patient consent for publication

Not applicable.

Competing interests

The authors declare that they have no competing interests.

References

1. Siegel RL, Miller KD, Fuchs HE and Jemal A: Cancer statistics, 2022. CA Cancer J Clin 72: 7-33, 2022.
2. He D, Wang D, Lu P, Yang N, Xue Z, Zhu X, Zhang P and Fan G: Single-cell RNA sequencing reveals heterogeneous tumor and immune cell populations in early-stage lung adenocarcinomas harboring EGFR mutations. Oncogene 40: 355-368, 2021.
3. Dong ZY, Zhang C, Li YF, Su J, Xie Z, Liu SY, Yan LX, Chen ZH, Yang XN, Lin JT, *et al*: Genetic and immune profiles of solid predominant lung adenocarcinoma reveal potential immunotherapeutic strategies. J Thorac Oncol 13: 85-96, 2018.
4. Schneider F and Dacic S: Histopathologic and molecular approach to staging of multiple lung nodules. Transl Lung Cancer Res 6: 540-549, 2017.
5. Bhan A, Soleimani M and Mandal SS: Long noncoding RNA and cancer: A new paradigm. Cancer Res 77: 3965-3981, 2017.
6. Yousefi H, Maheronnaghsh M, Molaei F, Mashouri L, Reza Aref A, Momeny M and Alahari SK: Long noncoding RNAs and exosomal lncRNAs: Classification, and mechanisms in breast cancer metastasis and drug resistance. Oncogene 39: 953-974, 2020.
7. Li SY, Zhu Y, Li RN, Huang JH, You K, Yuan YF and Zhuang SM: LncRNA Lnc-APUE is repressed by HNF4α and promotes G1/S phase transition and tumor growth by regulating MiR-20b/E2F1 axis. Adv Sci (Weinh) 8: 2003094, 2021.
8. Parasramka MA, Maji S, Matsuda A, Yan IK and Patel T: Long non-coding RNAs as novel targets for therapy in hepatocellular carcinoma. Pharmacol Ther 161: 67-78, 2016.
9. Chen HY, Chan SJ, Liu X, Wei AC, Jian RI, Huang KW, Lang YD, Shih JH, Liao CC, Luan CL, *et al*: Long noncoding RNA Smyca coactivates TGF-β/Smad and Myc pathways to drive tumor progression. J Hematol Oncol 15: 85, 2022.
10. Ma F, Liu X, Zhou S, Li W, Liu C, Chadwick M and Qian C: Long non-coding RNA FGF13-AS1 inhibits glycolysis and stemness properties of breast cancer cells through FGF13-AS1/IGF2BPs/Myc feedback loop. Cancer Lett 450: 63-75, 2019.
11. Livak KJ and Schmittgen TD: Analysis of relative gene expression data using real-time quantitative PCR and the 2(-Delta Delta C(T)) method. Methods 25: 402-408, 2001.
12. Venkatesh J, Wasson MD, Brown JM, Fernando W and Marcato P: LncRNA-miRNA axes in breast cancer: Novel points of interaction for strategic attack. Cancer Lett 509: 81-88, 2021.
13. Huang H, Yang C, Zhang Q, Zhuo T, Li X, Li N, Zhu L, Luo C, Gan J and Wu Y: Long non-coding RNA FAM83A antisense RNA 1 (lncRNA FAM83A-AS1) targets microRNA-141-3p to regulate lung adenocarcinoma cell proliferation, migration, invasion, and epithelial-mesenchymal transition progression. Bioengineered 13: 4964-4977, 2022.
14. Jiang J, Bi Y, Liu XP, Yu D, Yan X, Yao J, Liu T and Li S: To construct a ceRNA regulatory network as prognostic biomarkers for bladder cancer. J Cell Mol Med 24: 5375-5386, 2020.
15. Su L, Li R, Zhang Z, Liu J, Du J and Wei H: Identification of altered exosomal microRNAs and mRNAs in Alzheimer's disease. Ageing Res Rev 73: 101497, 2022.

16. Shi T, Ma Y, Cao L, Zhan S, Xu Y, Fu F, Liu C, Zhang G, Wang Z, Wang R, *et al*: B7-H3 promotes aerobic glycolysis and chemoresistance in colorectal cancer cells by regulating HK2. Cell Death Dis 10: 308, 2019.
17. Caso R, Sanchez-Vega F, Tan KS, Mastrogiacomo B, Zhou J, Jones GD, Nguyen B, Schultz N, Connolly JG, Brandt WS, *et al*: The underlying tumor genomics of predominant histologic subtypes in lung adenocarcinoma. J Thorac Oncol 15: 1844-1856, 2020.
18. Shi Q, Shao K, Jia H, Cao B, Li W, Dong S, Liu J, Wu K, Liu M, Liu F, *et al*: Genomic alterations and evolution of cell clusters in metastatic invasive micropapillary carcinoma of the breast. Nat Commun 13: 111, 2022.
19. Tavernari D, Battistello E, Dheilly E, Petruzzella AS, Mina M, Sordet-Dessimoz J, Peters S, Krueger T, Gfeller D, Riggi N, *et al*: Nongenetic evolution drives lung adenocarcinoma spatial heterogeneity and progression. Cancer Discov 11: 1490-1507, 2021.
20. Sato R, Imamura K, Semba T, Tomita Y, Saeki S, Ikeda K, Komohara Y, Suzuki M, Sakagami T, Saya H and Arima Y: TGFβ signaling activated by cancer-associated fibroblasts determines the histological signature of lung adenocarcinoma. Cancer Res 81: 4751-4765, 2021.
21. Zhang S, Xu Y, Zhao P, Bao H, Wang X, Liu R, Xu R, Xiang J, Jiang H, Yan J, *et al*: Integrated analysis of genomic and immunological features in lung adenocarcinoma with micropapillary component. Front Oncol 11: 652193, 2021.
22. Tang M, Abbas HA, Negrao MV, Ramineni M, Hu X, Hubert SM, Fujimoto J, Reuben A, Varghese S, Zhang J, *et al*: The histologic phenotype of lung cancers is associated with transcriptomic features rather than genomic characteristics. Nat Commun 12: 7081, 2021.
23. Nguyen TT, Lee HS, Burt BM, Wu J, Zhang J, Amos CI and Cheng C: A lepidic gene signature predicts patient prognosis and sensitivity to immunotherapy in lung adenocarcinoma. Genome Med 14: 5, 2022.
24. Chen Z, Hu Z, Sui Q, Huang Y, Zhao M, Li M, Liang J, Lu T, Zhan C, Lin Z, *et al*: LncRNA FAM83A-AS1 facilitates tumor proliferation and the migration via the HIF-1α/glycolysis axis in lung adenocarcinoma. Int J Biol Sci 18: 522-535, 2022.
25. Jia J, Li H, Chu J, Sheng J, Wang C, Jia Z, Meng W, Yin H, Wan J and He F: LncRNA FAM83A-AS1 promotes ESCC progression by regulating miR-214/CDC25B axis. J Cancer 12: 1200-1211, 2021.
26. He J and Yu J: Long noncoding RNA FAM83A-AS1 facilitates hepatocellular carcinoma progression by binding with NOP58 to enhance the mRNA stability of FAM83A. Biosci Rep 39: BSR20192550, 2019.
27. Wang W, Zhao Z, Xu C, Li C, Ding C, Chen J, Chen T and Zhao J: LncRNA FAM83A-AS1 promotes lung adenocarcinoma progression by enhancing the pre-mRNA stability of FAM83A. Thorac Cancer 12: 1495-1502, 2021.
28. Xiao G, Wang P, Zheng X, Liu D and Sun X: FAM83A-AS1 promotes lung adenocarcinoma cell migration and invasion by targeting miR-150-5p and modifying MMP14. Cell Cycle 18: 2972-2985, 2019.
29. Lunt SY and Vander Heiden MG: Aerobic glycolysis: Meeting the metabolic requirements of cell proliferation. Annu Rev Cell Dev Biol 27: 441-464, 2011.
30. Zhou L, Li M, Yu X, Gao F and Li W: Repression of hexokinases II-mediated glycolysis contributes to piperlongumine-induced tumor suppression in non-small cell lung cancer cells. Int J Biol Sci 15: 826-837, 2019.
31. Tantai J, Pan X, Chen Y, Shen Y and Ji C: TRIM46 activates AKT/HK2 signaling by modifying PHLPP2 ubiquitylation to promote glycolysis and chemoresistance of lung cancer cells. Cell Death Dis 13: 285, 2022.
32. Li X, Li Y, Bai S, Zhang J, Liu Z and Yang J: NR2F1-AS1/miR-140/HK2 axis regulates hypoxia-induced glycolysis and migration in hepatocellular carcinoma. Cancer Manag Res 13: 427-437, 2021.
33. Chen J, Yu Y, Li H, Hu Q, Chen X, He Y, Xue C, Ren F, Ren Z, Li J, *et al*: Long non-coding RNA PVT1 promotes tumor progression by regulating the miR-143/HK2 axis in gallbladder cancer. Mol Cancer 18: 33, 2019.
34. Yu T, Li G, Wang C, Gong G, Wang L, Li C, Chen Y and Wang X: MIR210HG regulates glycolysis, cell proliferation, and metastasis of pancreatic cancer cells through miR-125b-5p/HK2/PKM2 axis. RNA Biol 18: 2513-2530, 2021.